Nanoparticle assisted mechanical delamination for free-standing high performance organic devices

Silvia Colodrero[1], Pablo Romero-Gomez[1], Paola Mantilla-Perez[1] and Jordi Martorell[1,2*]*

[1]ICFO-Institut de Ciencies Fotoniques, The Barcelona Institute of Science and Technology, 08860 Castelldefels (Barcelona), Spain

[2]Departament de Física, Universitat Politecnica de Catalunya, Terrassa, Spain

E-mail: silvia.colodrero@icfo.es, jordi.martorell@icfo.es

Keywords: nanoparticles, sacrificial layer, photovoltaic performance, free-standing, organic solar cells.

Abstract. Organic electronics has the potential to be incorporated in any kind of surface morphology for wearable or fully portable applications. Unfortunately when organic devices, such as for instance solar cells, are fabricated on flexible substrates, the device performance is severely limited unless the physical properties of such substrates are carefully chosen. In here, we demonstrate that layers of nanoparticles with a size gradient distribution can be used to obtain high performance solar cell devices that can be effectively delaminated from an original flat and rigid glass substrate. We incorporated such sacrificial nanoparticles layers in between the glass substrate and the semi-transparent electrode of a PTB7:$PC_{71}BM$ cell. After the cell delamination, we obtained free-standing flexible devices with power conversion efficiencies as high as 7.12%, corresponding to 90% of the performance of the same cell fabricated on a standard glass smooth surface.

1. Introduction

A determining step towards a low cost printable electronics with the potential to be incorporated in portable or wearable flexible devices may be achieved once such devices can be fabricated on any kind of material surface.[1-4] Within this context, the unique properties of

polymer solar cells (PSCs) make them ideal candidates to become the electrical source to power up such type of electronic devices.[5-9] Indeed, it has been recently shown that high performance PSCs can be grown on smooth substrates made of flexible glass or different polymeric substrates after optimizing the optical and mechanical properties for either the transparent conductive electrode (TCE) or the absorbing layer.[10-16]

Unfortunately, the photovoltaic parameters rapidly degrade once substrate materials with a porosity or roughness that depart from the ideal for optimal solar cells are being used. In solution processed high performance polymer cells, the active material is composed of a donor acceptor bulk hetero-junction forming a blend.[7,8,17-20] High efficiency cells can be reached provided an optimal nano-morphology for such blend is obtained during the cell fabrication.[21-24] Indeed, any tiny disturbance in the fabrication procedure or an inappropriate substrate surface roughness may cause dramatic losses in the final device performance.[25] Fabricating photovoltaic devices on top of high quality smooth surfaces and subsequently transferring them onto the desired final surface has been applied successfully to different inorganic materials. In this case, the implementation of sacrificial coatings or the use of solvent assisted processes have demonstrated the effective delamination of gallium arsenide (GaAs), amorphous silicon (a-Si) or indium-gallium-phosphide (InGaP) cells, which exhibited similar efficiencies after the peeling process.[26-28] However, the delicate nature of the organic materials together with the relatively weak forces that glue them together within the blend or the adjacent layers in the cell architecture make such solutions used for inorganic cells impracticable for polymer ones.

In this paper we propose a new route to fabricate high performance polymer cells that can be transferred to any kind of substrates, regardless of its porosity. To do so, we incorporated a nanoparticle sacrificial layer, with a thickness equivalent to several particle diameters, in between a flat glass substrate and the first semi-transparent electrode of a polymer cell. It is

well known that van de Waals forces and capillary forces play a major role in the adhesion properties of nanoparticle systems.[29,30] We show here that, by adequately selecting the particle size and layer thickness, the overall effect of such forces is smaller than the interaction forces among all the layers forming the cell. Hence, crack formation along that sacrificial film may occur when mechanical strain is applied. On the other hand, to diminish the surface roughness of the nanoparticle layer in direct contact with the cell and cause a minimal disturbance to the blend nano-morphology, we implemented a large to small nanoparticle size gradient. Transferred and free-standing PSCs with efficiencies as high as 8.17% and 7.12%, respectively, were attained for PTB7:$PC_{71}BM$ active layers after an optimization of both the sacrificial layer and the TCE configuration. Comparatively, the performance of a reference cell containing the same nanoparticle film before the delamination process was 8.24%. In other words, with the nanoparticle assisted delamination, we were able to maintain close to 100% and 90% of the performance for transferred and free-standing cells, respectively.

2. Devices integrating nanoparticle sacrificial layers

A schematic illustration depicting the methodology proposed to fabricate transferred and free-standing PSCs through a mechanical peeling approach is shown in **Figure 1**. As indicated above, the main challenge herein consists in integrating a sacrificial layer made of nanoparticles, with the adequate surface roughness and porosity, in between the glass substrate and the TCE employed without affecting the main photovoltaic parameters of the device. An additional requirement to be solved concerns the fabrication of a TCE able to better withstand tensile strength than ITO.[31 - 33] This would ensure a good electrical performance after the peeling process. In this case, we implemented an electrode configuration based on a dielectric/metal/dielectric (DMD) multilayer. The ductile nature of the ultra-thin metallic layer provides an enhanced flexibility for those hybrid films. Moreover, the realization of such kind of electrodes has demonstrated a clear advantage in terms of cost-

effectiveness, compatibility with plastic materials and high throughput production at low processing temperatures.[10,13,34-39]

Taking all these considerations into account, the adhesion properties of several films made of both sol-gel precursor solutions and nanoparticle suspensions were first evaluated following the simple scotch tape test.[40] We compared that behaviour when using a sol-gel titanium dioxide (TiO_2) precursor, zinc oxide (ZnO) and aluminium oxide (Al_2O_3) nanoparticle suspensions with average size distributions centred at 10 nm and 30 nm, respectively. The results obtained after the peeling test showed that the film made of nanoparticles with a larger particle size, i.e. Al_2O_3, could be easily and almost completely released from the substrate. This is most likely related to the larger inherent surface roughness of that film and, subsequently, to the decreased area of contact between solid surfaces (see Supporting Information).

To estimate the impact that such layer could have on the device performance, PSCs constructed onto ZnO/Ag/ZnO electrodes with and without the nanoparticle film were prepared. We followed a protocol for the deposition of the multilayer electrode previously reported by Wang and co-workers.[13] Reference cells based on conventional ITO substrates were also prepared for comparison. As clearly observed in Figure 2a, slightly higher short circuit photocurrents (J_{SC}) were systematically reached when the DMD electrode was incorporated into the cell, whereas the fill factor (FF) and the open circuit voltage (V_{OC}) values were similar for the whole set except for the device that incorporated the Al_2O_3 under-layer. This dramatic decrease in the FF is attributed to the larger surface roughness of the nanoparticle film when compared to a standard substrate.[25,41] With the aim to reduce the roughness of the interface separating the sacrificial layer from the cell, a bi-layer structure in which fine nanoparticles, i.e ZnO, were deposited on top of the Al_2O_3 coating before the deposition of the electrode was prepared. We built in this way a large to small particle size

gradient to minimize any detrimental effect on the blend nano-morphology. After that we obtained, as seen in Figure 2a, a FF similar to the one from the reference cells and, consequently, comparable power conversion efficiency (PCE) for the devices incorporating the sacrificial layer. Figure 2b shows the different transmittance spectra measured for both commercial ITO and the so fabricated ultrathin silver electrodes, denoted as ZAOZ from now on. Note that the loss in transmission due to the ZnO absorption for wavelengths below 400 nm when compared to that of ITO does not have a detrimental effect on the cell performance since the contribution of photons at that spectral range only accounts for around 2% of the total solar spectrum irradiance. We have also included in this graph the transmittance spectra corresponding to the films of ZnO and Al_2O_3 nanoparticles deposited onto glass substrates. The high transparency of those layers is essential to allow photons to reach the active layer when partially remaining on top of the device after the delamination process.

The surface roughness and topography corresponding to the single and bi layers were further investigated by atomic force microscopy (AFM). From Figure 3b-3d we obtained root mean square (RMS) roughness values of 2.6 nm, 1.9 nm and 1.4 nm for the Al_2O_3 nanoparticle layer, the Al_2O_3/ZnO nanoparticle bi-layer and the final assembly Al_2O_3/ZnO/ZAOZ, respectively. Although the surface roughness for the latter structure was somewhat larger than the one measured for the bare ZAOZ, with a value of 0.32 nm (cf. Figure 3a), it was comparable to the roughness value of commercial ITO (1.2 nm). In combination with the results presented in Figure 2a, one may conclude that surface roughness value approximately below 1.5 nm does not have any detrimental effect on the device performance regardless of the TCE employed. Also, by comparing Figure 3b-3d, it can be noted that the morphology of the porous Al_2O_3 nanoparticle film becomes denser and more compact after the deposition of the ZnO nanoparticles and the ZAOZ electrode. However, the granular shape resembling the first layer is clearly maintained after the fabrication of the latter ones.

3. Nanoparticle assisted mechanical delamination

To carry out the delamination process of the entire device, we made use of a photo-curable polymeric compound to cover the upper part of the cells. Such compound acted at the same time as a glue with strong enough adhesion to an acceptor glass placed at the cell backside as to favour, under mechanical stress, crack propagation along the nanoparticle film. Analogous approaches can be also found in the literature for the peeling of simple optical elements.[42,43] In our case, when implementing the detachment procedure, a minimum thickness for the nanoparticle film is required for the complete peeling of the cells, otherwise the delamination process would occur somewhere else within the device. After trying many different combinations, we found optimal thicknesses of approximately 140 nm and 40 nm for the Al_2O_3 and the ZnO layers, respectively. Additionally, the weak adhesion between the ZAOZ and the active layer led in many occasions to an incomplete peeling of the cells. To overcome this issue, the thicknesses for the ZAOZ electrode were modified to be 50/7/12 nm instead of 50/7/50 nm, while an extra 30 nm sol gel ZnO blocking layer was added on top. By doing so, the total thickness for the upper ZnO layer constituting the TCE was essentially unaltered while the electrode-active layer adhesion was greatly improved.

Again, the ZAOZ based PSC with the optimized underneath layer exhibited a better performance when compared to the ITO reference cell due to its higher J_{SC}, as seen in Figure 4a. From the external quantum efficiency (EQE) curves shown in Figure 4b, we observe that the two characteristic peaks at 450 nm and 650 nm, corresponding to the acceptor and donor absorption maxima, respectively, are enhanced when the ZAOZ electrode is used to replace the standard ITO. Such improvement can be ascribed to an optical resonance resulting from the cavity formed by the two metallic electrodes.[13] However, the additional dielectric layers that compose the ZAOZ electrode may also play a relevant role in the overall electromagnetic field absorption that needs to be further analyzed. Finally, the removal of the substrate in the

detached cell leads to a similar EQE shape with an enhanced increase in photon absorption clearly visible in the 400-550 nm wavelength range. This increase may be less apparent at some other wavelength ranges due to the presence of some nanoparticles that still remain on the cell surface after the detachment procedure is completed.

4. Free-standing high efficiency devices

We followed a similar methodology to obtain free-standing devices, supported this time only by the thin layer of polymeric compound. In this case, a glass piece previously covered with a cured thin layer of silicon based organic polymer, such as polydimethylsiloxane (PDMS), was employed as the acceptor substrate. Since the interaction forces present at the interface between the two polymeric compounds, i.e. the epoxy resin and the PDMS, were still stronger than the adhesion force of the nanoparticles to the supporting substrate, this procedure allowed us to efficiently separate the whole set of layers from it. This was further assisted during the UV light epoxy resin curing process, which also made PDMS more hydrophilic. Once the cell was completely released from the substrate, the PDMS covered glass slide could be separated to give rise to a free-standing flexible device. Figure 5 shows the J-V curve for the free-standing cell together with some images showing both the appearance and the analysis of its cross section taken by scanning electron microscopy (SEM). From the latter, one may see that some nanoparticles are lifted together with the cell after the separation process. Those nanoparticles, with a thickness of around 100 nm after the peeling, could also serve as an antireflection coating when appropriate optical parameters are considered. The inset picture from Figure 5a illustrates the high transparency of the epoxy resin layer supporting the cell. Since such polymeric compounds are generally employed to encapsulate optoelectronic components, they may also provide a good moisture and solvent protection to the cell. Highly flexible cells should be reasonably easy to achieve by thinning down to a few hundreds of nanometers the thickness of such polymeric compound. Given that all cell layers

possess inherently such property,[10,13,38] the challenge in obtaining cells with a high degree of flexibility rests on finding the optimal epoxy layer thickness adequately balancing barrier properties with bendability.

Average values with standard deviations of the photovoltaic parameters extracted from the J-V curves for the fabricated devices are summarized in Table 1. In parentheses are depicted the results corresponding to the best device performance. A slightly lower FF was obtained for the transferred and free-standing PSCs as a consequence of the strain caused during the peeling process, whereas the V_{OC} was practically unaltered for the former when compared to the reference cell. As discussed above, higher J_{SC} were attained for the cell configurations in which the frontal substrate was removed. As a result, the efficiency of the transferred cell was equivalent to that measured with the supporting glass and incorporating the sacrificial nanoparticle layer. Similarly, the free-standing device kept almost 90% of its initial efficiency value.

5. Conclusion

In conclusion, we have developed a new transfer method, compatible with the delicate nano-morphology of organic semiconductors blends, by implementing a nanoparticle sacrificial layer with weak binding forces within the device configuration. We demonstrated that a large to small nanoparticle size gradient for the sacrificial layer can reduce the impact on the cell nano-morphology. This allows overcoming one of the major challenges within the field concerning the fabrication of flexible solar cells with no restriction in terms of thermal processing or morphological properties of the substrate. A precise optimization of, both, the nanoparticle film and the transparent conductive electrode led to transferred and free-standing PTB7:PC_{71}BM cells with efficiencies as high as 8.17% and 7.12%, respectively. The remarkable high efficiency achieved for the free-standing cells may give rise to devices

adaptable to any kind of surface, which are completely suitable for integration in wearable or fully portable electronics. Further developments should focus on the accomplishment of devices with higher degrees of adaptability and stability by means of selecting the adequate supporting and encapsulating polymeric configurations, whereas no change on the cell architecture would be, in principle, required. Indeed, determining the adequate thickness of the epoxy resin to provide an optimal balance between barrier properties and bendability remains as one of the major challenges for future work.

6. Experimental section

Sol gel and nanoparticle precursors: All commercially available chemicals were employed without any further purification. For the sol gel TiO_2 solution, 350 µl of titanium tetraisopropoxide ($Ti[OCH(CH_3)_2]_4$, Sigma Aldrich 97%) were slowly added to a vial containing 5 ml of ethanol (Scharlau, 99.5%) and 100 ml of 1 M hydrochloric acid solution (Fluka) while stirring. The sol gel ZnO solution was prepared by dissolving 400 mg of zinc acetate dehydrate ($Zn(CH_3COO)_2 \cdot 2H_2O$, Sigma Aldrich 99.9%) and 111 µl of ethanolamine ($NH_2CH_2CH_2OH$, Sigma Aldrich 99.5%) in 6 ml of 2-methoxyethanol ($CH_3OCH_2CH_2OH$, Sigma Aldrich 99.8%) under stirring for at least 12 h. The nanoparticle suspensions of ZnO and Al_2O_3 were acquired from Nanograde® and Aldrich, respectively, and were diluted if necessary to get the required film thicknesses.

TCE fabrication method: Commercial ITO ($15 \Omega sq^{-1}$, Stuttgart) covered glass substrates were purchased from the Institute for Large Area Microelectronics (IGM). ZAOZ electrodes were deposited on glass substrates (Eagle XG, Corning glass) by multi-magnetron multi-gun sputtering (ATC Orion 8, AJA International Company). The ZnO sputtering process was carried out at radio frequency power of 50 W at room temperature using a 2 inch ZnO target (Kurt J. Lesker Company). The working pressure was kept at 3 mTorr by introducing pure Ar gas and the chamber was evacuated to a base pressure of $2x10^{-6}$ Torr before the deposition.

The AgO_x film was deposited via a dc reactive sputtering process, with a power of 18 W and using a 2 inch Ag target in reactive atmosphere (20 sccm Ar, 1 sccm O_2).

Optical and structural characterization: The optical transmission of the films was measured over the wavelength range of interest using a UV-vis-NIR spectrometer (Lambda 950, PerkinElmer) and keeping the samples under normal incident illumination conditions. The surface morphology of the films was evaluated from the average values of at least three different surface (1µm x 1µm) domains by tapping mode AFM (Dimension 3100, Veeco). The cross section morphology of the cells was checked by FEG-SEM (FEI Inspect F50-EBL).

PSC fabrication and photovoltaic characterization: We employed an inverted cell configuration as follows: TCE/ZnO/active layer/MoO_x/Ag.[44] For the ITO reference cells, the sol gel ZnO solution was first spin coated (WS-650Mz-23NPPB, Laurell Technologies) onto the previously cleaned substrates at a rotation speed of 5000 rpm and annealed at 180 ºC for 10 minutes. The samples were then transferred into a glovebox for next fabrication steps. Both the conjugated polymer and the fullerene derivative were purchased from 1-Material and used as received. A mixture of PTB7:$PC_{71}BM$ was prepared at a concentration of 10 mg/ml (1:1.5) in chlorobenzene and was kept under stirring overnight at 60 ºC. 1,8-diiodooctane (98%, Sigma Aldrich) was added in a volume ratio of 3% to the solution one hour before the active layer deposition. Then, it was deposited by spin coating at a rotation speed of 1400 rpm, adjusted to get the optimal 90 nm thickness, and was left to dry in vacuum for 1 hour, followed by the evaporation of MoO_x (5 nm) and Ag (120 nm). The same procedure was repeated for the case of the above detailed ZAOZ electrodes fabricated onto glass substrates. For the case of those cells integrating the nanoparticle sacrificial layer, thicknesses for the Al_2O_3 and ZnO films of 140 nm and 40 nm were employed and stabilized at 180 ºC during 10 min before the deposition of the rest of layers forming the device. The UV adhesive (ELC-4007) was purchased from Electro-lite Corporation and cured using an UVO-Cleaner (42A-220, Jelight Company) for 3 minutes.

The PCE of the fabricated solar cells was determined using an AM 1.5G solar simulator (Sun 3000, Abet Technologies) and a 100 $mWcm^{-2}$ illumination intensity, which was adjusted with a monocrystalline silicon reference cell (Hamamatsu) calibrated at the Fraunhofer Institute for Solar Energy Systems. The J-V curves were recorded using a Keithley 2400 SourceMeter. EQE values were measured using a quantum efficiency measurement system (QEX10, PV Measurements). In this case, the devices were illuminated using a monochromatic light coming from a xenon lamp. The spectral response of the calibrated silicon cell was used as a reference.

Supporting Information

Supporting Information is available from the Wiley Online Library or from the author.

Acknowledgments

We acknowledge financial support from the Spanish MINECO (Severo Ochoa program, grant No.: SEV-2015-0522), the MINECO and the Fondo Europeo de Desarrollo Regional FEDER (grant No.: MAT2014-52985-R), and the Fundacio Privada Cellex.

Table 1. Average PV parameters and standard deviations extracted from the analysis of the J-V curves for the fabricated devices (in parentheses PV parameters of the best devices).

Device	Jsc (mA/cm^2)	Voc (mV)	FF (%)	PCE (%)
ITO reference	14.1±0.21 (14.33)	732±0.26 (733)	72±1.08 (73)	7.4±0.21 (7.67)
ZAOZ reference	14.5±0.26 (14.77)	730±1.04 (730)	72±1.12 (71)	7.4±0.24 (7.65)
NP-ZAOZ	14.6±0.19 (14.79)	682±0.96 (681)	49±1.21 (50)	4.8±0.34 (5.04)
bi-NP ZAOZ	14.9±0.28 (15.02)	739±1.38 (742)	71±2.64 (74)	8.1±0.23 (8.24)
ZAOZ transferred	15.6±0.36 (15.73)	737±2.74 (742)	68±1.72 (70)	7.9±0.32 (8.17)
ZAOZ free-standing	15.1±0.6 (15.70)	727±3.12 (731)	59±3.37 (62)	6.9±0.12 (7.12)

References

[1] K. Nomura, H. Ohta, A. Takagi, T. Kamiya, M. Hirano, H. Hosono, *Nature* **2004**, *432*, 488.

[2] Y. G. Sun, J. A. Rogers, *Adv. Mater.* **2007**, *19*, 1897.

[3] L. B. Hu, M. Pasta, F. La Mantia, L. F. Cui, S. Jeong, H. D. Deshazer, J. W. Choi, S. M. Han, Y. Cui, *Nano Lett.* **2010**, *10*, 708.

[4] L. Li, Z. Wu, S. Yuan, X. B. Zhang, *Energy Environ. Sci.* **2014**, *7*, 2101.

[5] F. C. Krebs, S. A. Gevorgyan, J. Alstrup, *J. Mater. Chem.* **2009**, *19*, 5442.

[6] B. Kippelen, J. L. Bredas, *Energy Environ. Sci.* **2009**, *2*, 251.

[7] J. D. Chen, C. H. Cui, Y. Q. Li, L. Zhou, Q. D. Ou, C. Li, Y. F. Li, J. X. Tang, *Adv. Mater.* **2015**, *27*, 1035.

[8] Z. C. He, B. Xiao, F. Liu, H. B. Wu, Y. L. Yang, S. Xiao, C. Wang, T. P. Russell, Y. Cao, *Nature Photon.* **2015**, 9, 174.

[9] A. B. Yusoff, D. Kim, H. P. Kim, F. K. Shneider, W. J. da Silva, J. Jang, *Energy Environ. Sci.* **2015**, *8*, 303.

[10] N. Formica, P. Mantilla-Perez, D. S. Ghosh, D. Janner, T. L. Chen, M. H. Huang, S. Garner, J. Martorell, V. Pruneri, *ACS Applied Materials & Interfaces* **2015**, *7*, 4541.

[11] W. J. da Silva, H. P Kim, A. R. B. Yusoff, J. Jang, *Nanoscale* **2013**, *5*, 9324.

[12] L. Mao, Q. Chen, Y. W. Li, Y. Li, J. H. Cai, W. M. Su, S. Bai, Y. Z. Jin, C. Q. Ma, Z. Cui, L. W. Chen, *Nano Energy* **2014**, *10*, 259.

[13] W. Wang, M. Song, T. S. Bae, Y. H. Park, Y. C. Kang, S. G. Lee, S. Y. Kim, D. H. Kim, S. Lee, G. H. Min, G. H. Lee, J. W. Kang, J. Yun, *Adv. Funct. Mater.* **2014**, *24*, 1551.

[14] M. Song, J. H. Park, C. S. Kim, D. H. Kim, Y. C. Kang, S. H. Jin, W. Y. Jin, J. W. Kang, *Nano Research* **2014**, *7*, 1370.

[15] J. H. Seo, H. D. Um, A. Shukla, I. Hwang, J. Park, Y. C. Kang, C. S. Kim, M. Song, K. Seo, *Nano Energy* **2015**, *16*, 122.

[16] T. Kim, J. H. Kim, T. E. Kang, C. Lee, H. Kang, M. Shin, C. Wang, B. Ma, U. Jeong, T. S. Kim, B. J. Kim, *Nat. Commun.* **2015**, *6*, 8547.

[17] G. Li, V. Shrotriya, J. S. Huang, Y. Yao, T. Moriarty, K. Emery, Y. Yang, *Nat. Mater.* **2005**, *4*, 864.

[18] B. C. Thompson, J. M. J. Frechet, *Angew. Chem. Int. Edit.* **2008**, *47*, 58.

[19] H. Y. Chen, J. H. Hou, S. Q. Zhang, Y. Y. Liang, G. W. Yang, Y. Yang, L. P. Yu, Y. Wu, G. Li, *Nature Photon.* **2009**, 3, 649.

[20] Y. Y. Liang, Z. Xu, J. B. Xia, S. T. Tsai, Y. Wu, G. Li, C. Ray, L. P. Yu, *Adv. Mater.* **2010**, *22*, E135.

[21] X. N. Yang, J. Loos, S. C. Veenstra, W. J. H. Verhees, M. M. Wienk, J. M. Kroon, M. A. J. Michels, R. A. J. Janssen, *Nano Lett.* **2005**, *5*, 579.

[22] H. Hoppe, N. S. Sariciftci, *J. Mater. Chem.* **2006**, *16*, 45.

[23] S. H. Park, A. Roy, S. Beaupre, S. Cho, N. Coates, J. S. Moon, D. Moses, M. Leclerc, K. Lee, A. J. Heeger, *Nature Photon.* **2009**, *3*, 297.

[24] M. He, M. Y. Wang, C. J. Lin, Z. Q. Lin, *Nanoscale* **2014**, *6*, 3984.

[25] J. R. Tumbleston, A. Gadisa, Y. C. Liu, B. A. Collins, E. T. Samulski, R. Lopez, H. Ade, *ACS Applied Materials & Interfaces* **2013**, *5*, 8225.

[26] C. H. Lee, D. R. Kim, X. L. Zheng, *Nano Lett.* **2011**, *11*, 3435.

[27] C. H. Lee, D. R. Kim, I. S. Cho, N. William, Q. Wang, X. L. Zheng, *Scientific Reports* **2012**, *2*, 1000.

[28] C. H. Lee, D. R. Kim, X. L. Zheng, *ACS Nano* **2014**, *8*, 8746.

[29] Y. J. Min, M. Akbulut, K. Kristiansen, Y. Golan, J. Israelachvili, *Nat. Mater.* **2008**, *7*, 527.

[30] S. M. You, M. P. Wan, *Langmuir* **2013**, *29*, 9104.

[31] D. R. Cairns, R. P. Witte, D. K. Sparacin, S. M. Sachsman, D. C. Paine, G. P. Crawford, R. R. Newton, *Appl. Phys. Lett.* **2000**, *76*, 1425.

[32] Z. Chen, B. Cotterell, W. Wang, E. Guenther, S. J. Chua, *Thin Solid Films* **2001**, *394*, 202.

[33] S. K. Park, J. I. Han, D. G. Moon, W. K. Kim, *Jpn. J. Appl. Phys.*, Part 1 **2003**, *42*, 623.

[34] C. Guillen, J. Herrero, *Thin Solid Films* **2011**, *520*, 1.

[35] H. Han, N. D. Theodore, T. L. Alford, *J. Appl. Phys.* **2008**, *103*, 013708.

[36] N. P. Sergeant, A. Hadipour, B. Niesen, D. Cheyns, P. Heremans, P. Peumans, B. P. Rand, *Adv. Mater.* **2012**, *24*, 728.

[37] S. Schubert, M. Hermenau, J. Meiss, L. Müller-Meskamp, K. Leo, *Adv. Funct. Mater.* **2012**, *22*, 4993.

[38] D. S. Ghosh, Q. Liu, P. Mantilla-Perez, T. L. Chen, V. Mkhitaryan, M. H. Huang, S. Garner, J. Martorell, V. Pruneri, *Adv. Funct. Mater.* **2015**, *25*, 7309.

[39] F. Pastorelli, P. Romero-Gomez, R. Betancur, A. Martinez-Otero, P. Mantilla-Perez, N. Bonod, J. Martorell, *Adv. Energy Mater.* **2015**, *5*, 1400614.

[40] Standard Test Methods for Measuring Adhesion by Tape Test, ASTM D3359-09e2 (ASTM International) **2009**, West Conshohocken, PA.

[41] Z. F. Ma, Z. Tang, E. G. Wang, M. R. Andersson, O. Inganas, F. L. Zhang, *J. Phys. Chem. C* **2012**, *116*, 24462.

[42] M. E. Calvo, O. S. Sobrado, G. Lozano, H. Míguez, *J. Mater. Chem.* **2009**, *19*, 3144.

[43] M. E. Calvo, L. González-García, J. Parra-Barranco, A. Barranco, A. Jiménez-Solano, A. R. González-Elipe, H. Míguez, *Adv. Optical Mater.* **2015**, *3*, 171.

[44] P. Romero-Gomez, R. Betancur, A. Martinez-Otero, X. Elias, M. Mariano, B. Romero, B. Arredondo, R. Vergaz, J. Martorell, *Sol. Energ. Mat. Solar Cells* **2015**, *137*, 44.

Figure captions

Figure 1. (a) Conventional architecture of a typical cell deposited on an ITO substrate. (b) Modified design of the cell integrating a sacrificial layer made of nanoparticles and a DMD electrode. (c) Separation process of the so fabricated devices to obtain transferred or free-standing PSCs.

Figure 2. (a) J-V characteristic curves for ITO (blue line) and ZAOZ (red line) reference cells, and the devices integrating a single Al_2O_3 nanoparticle film (dotted grey line) and a smoothened nanoparticle bi-layer (black line). (b) Optical transmittance spectra corresponding to the commercial ITO (blue line) and the ZAOZ (red line) electrodes with thicknesses of 100 nm and 50/7/50 nm, respectively. For comparison, the transmittance of Al_2O_3 (grey line) and ZnO (black line) nanoparticle films are also shown.

Figure 3. (a)-(d) AFM images corresponding to the bare ZAOZ electrode, the Al_2O_3 nanoparticle layer, the Al_2O_3/ZnO nanoparticle bi-layer and the final assembly Al_2O_3/ZnO/ZAOZ, respectively.

Figure 4. (a) J-V characteristic curves and (b) EQE curves measured for an ITO reference cell (blue line), a ZAOZ cell fabricated onto the Al_2O_3/ZnO nanoparticle bi-layer (red line), and the transferred cell (grey line), respectively. The inset simplified schemes illustrate light impinging first on the glass substrate side for the first two kinds of devices displayed, and the nanoparticle layer side for the last one.

Figure 5. (a) J-V characteristic curve for the free-standing PSC developed in this paper. Inset picture illustrates the high transparency of the epoxy resin layer supporting the cell. (b) SEM cross section image of the cell architecture with remaining nanoparticles at the frontal side.

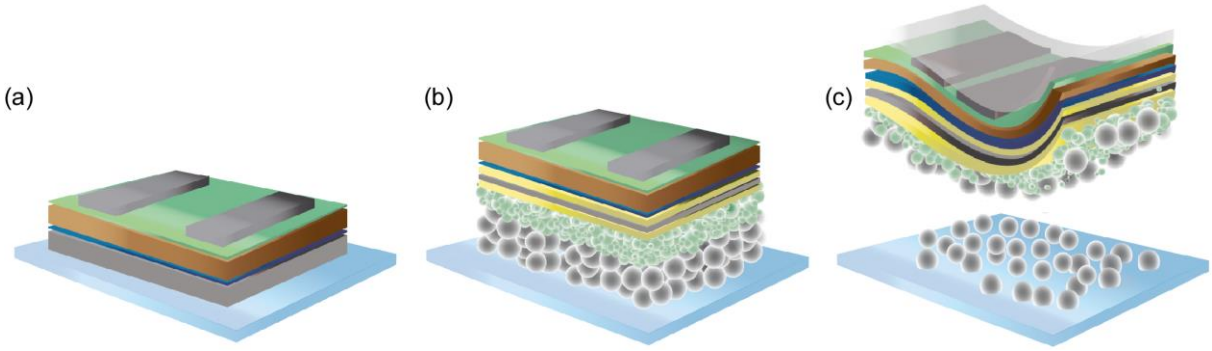

Figure 1. (a) Conventional architecture of a typical cell deposited on an ITO substrate. (b) Modified design of the cell integrating a sacrificial layer made of nanoparticles and a DMD electrode. (c) Separation process of the so fabricated devices to obtain transferred or free-standing PSCs.

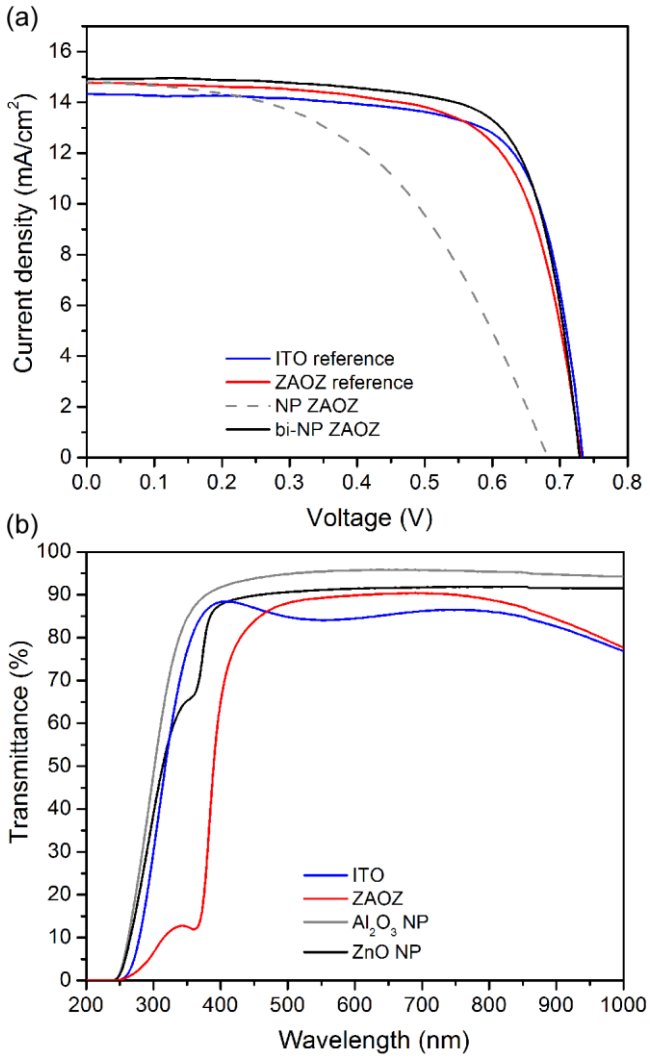

Figure 2. (a) J-V characteristic curves for ITO (blue line) and ZAOZ (red line) reference cells, and the devices integrating a single Al_2O_3 nanoparticle film (dotted grey line) and a smoothened nanoparticle bi-layer (black line). (b) Optical transmittance spectra corresponding to the commercial ITO (blue line) and the ZAOZ (red line) electrodes with thicknesses of 100 nm and 50/7/50 nm, respectively. For comparison, the transmittance of Al_2O_3 (grey line) and ZnO (black line) nanoparticle films are also shown.

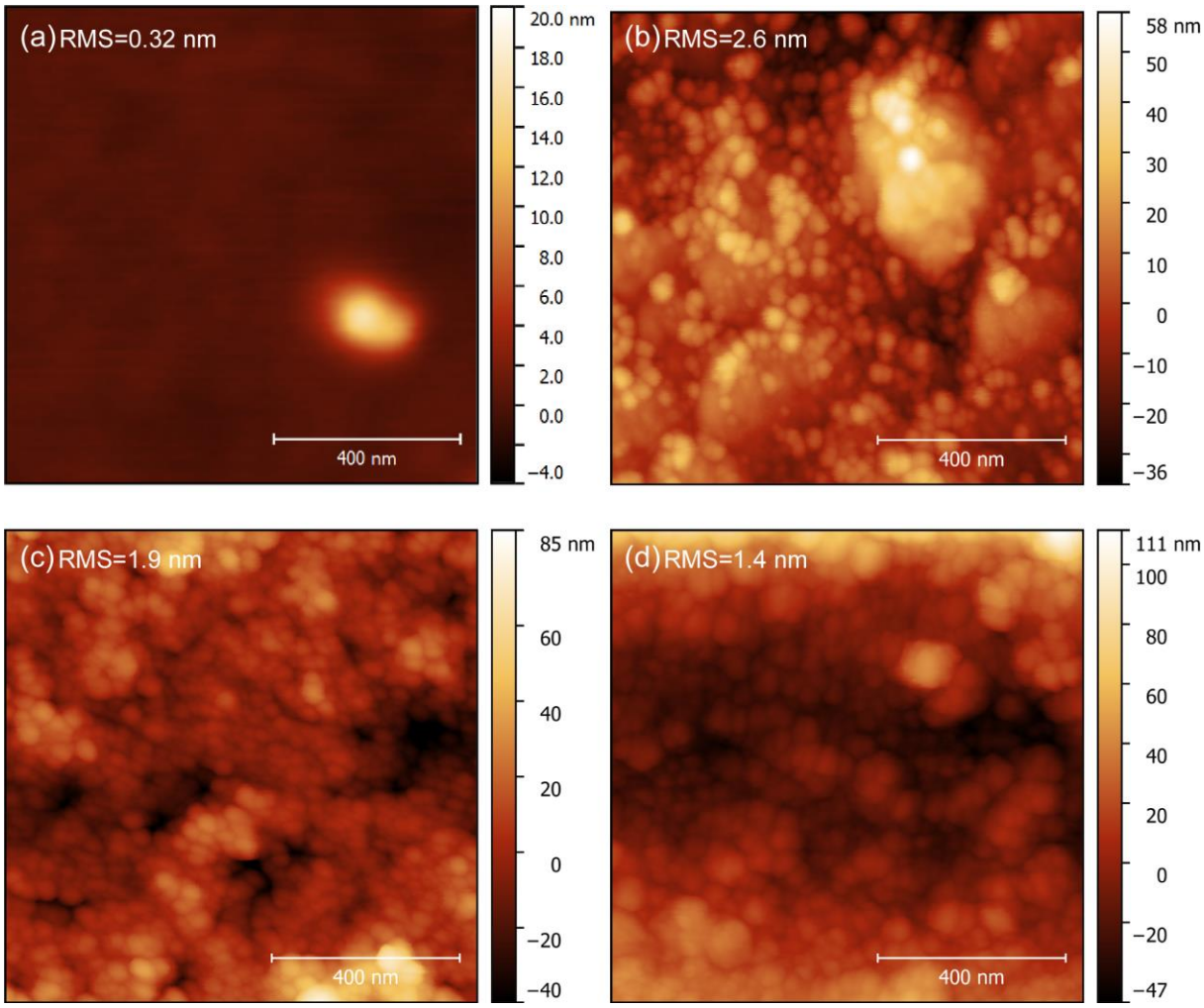

Figure 3. (a)-(d) AFM images corresponding to the bare ZAOZ electrode, the Al_2O_3 nanoparticle layer, the Al_2O_3/ZnO nanoparticle bi-layer and the final assembly Al_2O_3/ZnO/ZAOZ, respectively.

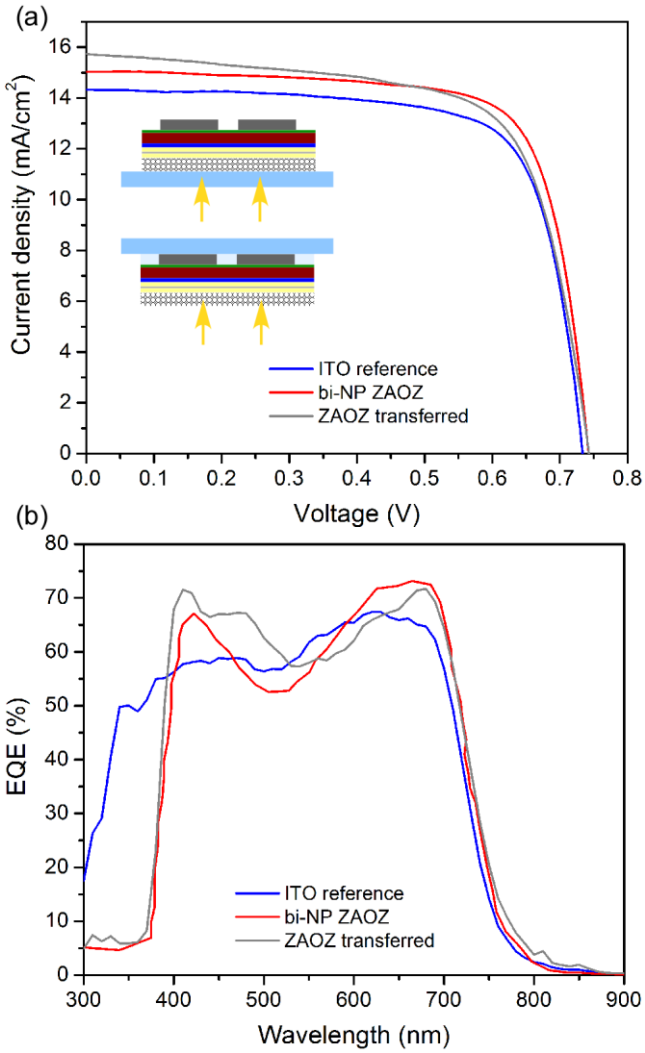

Figure 4. (a) J-V characteristic curves and (b) EQE curves measured for an ITO reference cell (blue line), a ZAOZ cell fabricated onto the Al_2O_3/ZnO nanoparticle bi-layer (red line), and the transferred cell (grey line), respectively. The inset simplified schemes illustrate light impinging first on the glass substrate side for the first two kinds of devices displayed, and the nanoparticle layer side for the last one.

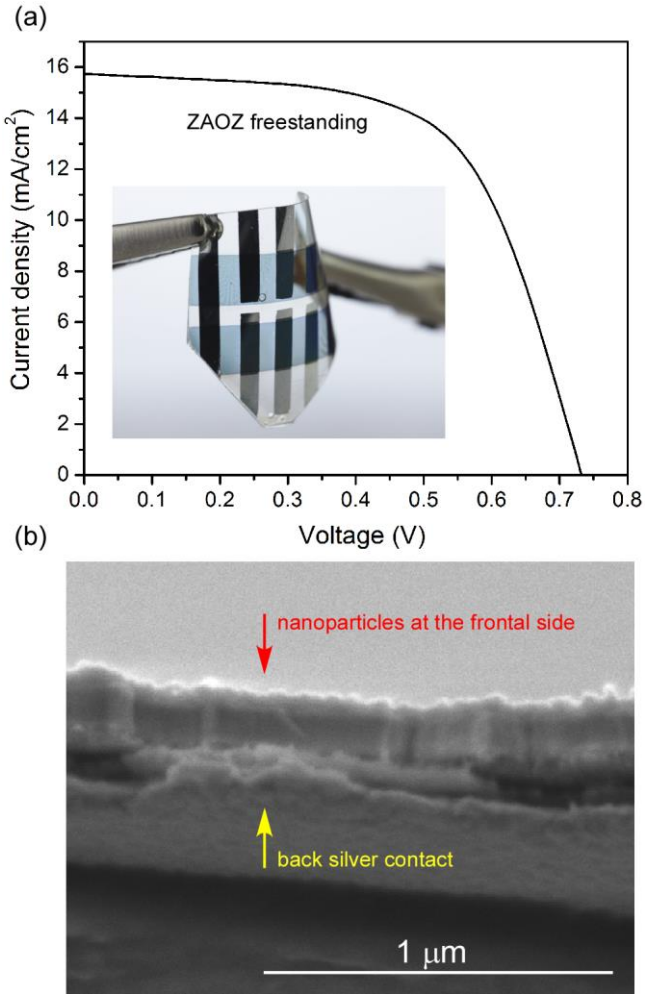

Figure 5. (a) J-V characteristic curve for the free-standing PSC developed in this paper. Inset picture illustrates the high transparency of the epoxy resin layer supporting the cell. (b) SEM cross section image of the cell architecture with remaining nanoparticles at the frontal side.